Available online at www.sciencedirect.com
ScienceDirect
Ceramics International 36 (2010) 1581–1588
CERAMICS INTERNATIONAL
www.elsevier.com/locate/ceramint

Rheology and pressure filtration of aqueous SiC suspensions of nanometer-sized bimodal particles

Naoki Matsunaga, Yuki Nakashima, Yoshihiro Hirata *, Soichiro Sameshima

Department of Chemistry, Biotechnology, and Chemical Engineering, Kagoshima University, 1-21-40 Korimoto, Kagoshima 890-0065, Japan

Received 14 December 2009; received in revised form 15 January 2010; accepted 12 February 2010
Available online 9 March 2010

Abstract

The consolidation behavior of mixed SiC particles (30 and 800 nm diameters) at pH 7 was examined using a developed pressure filtration apparatus at a constant crosshead speed of a piston. The addition of 30 nm SiC to 800 nm SiC changed the rheological properties of colloidal suspension from Newtonian to pseudoplastic flow through Bingham flow with increasing amount of 30 nm SiC. A phase transition from a well dispersed suspension to a flocculated suspension occurred when the applied pressure exceeded a critical pressure (ΔP_{tc}). The ΔP_{tc} value decreased with increasing amount of 30 nm SiC. The packing density of bimodal SiC particles was analyzed based on the partial molar volume of each powder. The larger particles were more densely packed than the smaller particles in the mixed powder compact.

Keywords: A. Mixing; A. Slip casting; A. Suspensions; B. Porosity; D. SiC

1. Introduction

Pressure filtration can reduce the consolidation time of a colloidal suspension of nanometer-sized particles with high filtration resistance as compared with the filtration method using a gypsum mold. In our previous papers [1–3], the consolidation behavior of aqueous suspensions of hydroxyapatite, silicon carbide, 8 mol% yttria-stabilized zirconia, and alpha alumina powders in a size range from 20 to 800 nm was analyzed using a newly-developed pressure filtration apparatus at a constant pressure or at a constant crosshead speed of piston. From a comparison between applied pressure (ΔP_t) at a constant crosshead speed and volume of dehydrated filtrate (V_f), it was found that a phase transition from a dispersed state to a flocculated state occurs at a critical applied pressure (ΔP_{tc}). Based on the colloidal phase transition, a new filtration theory was developed to explain the $\Delta P_t - h_t$ (height of piston) relation for a flocculated suspension [4,5]. Good agreement was shown between the theory developed and experimental results of electrostatically-stabilized suspensions. Our next interest is to study the consolidation behavior of bimodal particles system. The quantitative analysis of the degree of particle mixing in two-component powder compacts is important to understand the sintering behavior, mechanical properties or electrical properties of the composite materials such as Al_2O_3–ZrO_2 [6], Al_2O_3–TiC [7], Al_2O_3–Ni [8], $3Al_2O_3{\cdot}2SiO_2$–$ZrO_2{\cdot}SiO_2$ [9] or Al_2O_3–ITO (indium tin oxide) [10–12]. In a two-component system of A–B, three types of particle contact of A–A, A–B and B–B are formed in the microstructure of the powder compact [13,14]. The particle connection provides the geometrical feature of the microdomain. In this paper, the rheological properties and consolidation behavior of bimodal SiC particles (30 and 800 nm diameters) at pH 7 were examined and the resultant packing density was analyzed using partial molar volumes of fine and large particles.

2. Fractional collision frequency and DLVO theory of SiC suspension

When the motion of colloidal particles is dominated by diffusion, Smoluchowski has given Eq. (1) for the number (b_{ij}) of collisions per unit time for any particles in the system [15],

$$b_{ij} = 4\pi C_i C_j D_i r_i (r_i + r_j)\left(\frac{1}{r_i} + \frac{1}{r_j}\right) = 4\pi C_i C_j D_i r_i \left\{4 + \left[\left(\frac{r_i}{r_j}\right)^{1/2} - \left(\frac{r_j}{r_i}\right)^{1/2}\right]^2\right\} \quad (1)$$

* Corresponding author. Tel.: +81 99 285 8325; fax: +81 99 257 4742.
E-mail address: hirata@apc.kagoshima-u.ac.jp (Y. Hirata).

0272-8842/$36.00
doi:10.1016/j.ceramint.2010.02.020

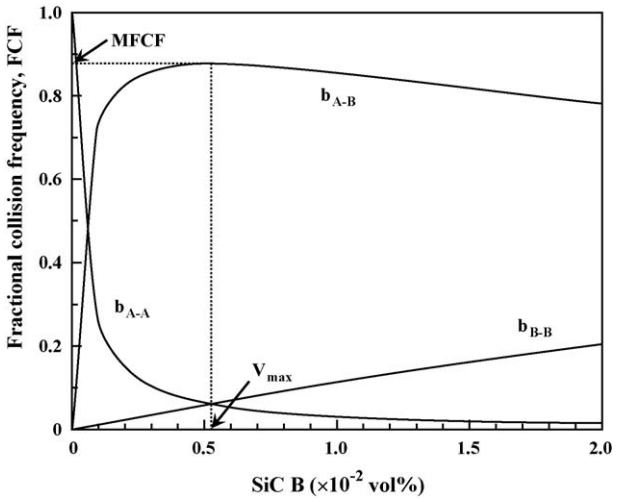

Fig. 1. Fractional collision frequency for bimodal particles system of 800 nm SiC (SiC A)–30 nm SiC (SiC B).

where C_i, D_i and r_i are the particle number concentration, diffusion coefficient and radius of i particle, respectively. The diffusion coefficient is inversely proportional to the radius of particle, as indicated by the Stokes' law ($D = kT/6\pi\eta r$, k: Boltzmann constant, η: viscosity). Collision frequency has a minimum at $r_i = r_j$ and becomes higher at larger difference of particle sizes. The fractional collision frequency between particles i and j, $(FCF)_{ij}$, is defined by Eq. (2).

$$(FCF)_{ij} = \frac{b_{ij}}{b_{ii} + 2b_{ij} + b_{jj}} \tag{2}$$

Fig. 1 shows the fractional collision frequency of the bimodal SiC particles system with $r_{\mathrm{SiC\ A}} = 400$ nm and $r_{\mathrm{SiC\ B}} = 15$ nm. The collision frequency of SiC A–SiC A particles decreases drastically with the addition of SiC B particles. The fractional collision frequency of SiC A–SiC B particles increases rapidly to 0.878 at SiC B fraction of 5.2×10^{-3} vol% vol% and decreases gradually at a higher SiC B fraction. The collision of SiC B–SiC B particles is also accelerated with the increase of SiC B fraction. The maximum fractional collision frequency ($MFCF$) and corresponding volume fraction (V_{max}) of SiC B for the collision of SiC A–SiC B are presented by Eqs. (3) and (4), respectively [14],

$$MFCF = \frac{(1+x)^2}{(1+x)^2 + 4x} \tag{3}$$

$$V_{\max} = \frac{1}{1+x^3} \tag{4}$$

where x is the particle size ratio of r_{A} (large particle)/r_{B} (small particle). The substitution of $x = 400$ nm/15 nm = 26.67 for Eqs. (3) and (4) results in $MFCF = 0.878$ and $V_{max} = 5.27 \times 10^{-3}$ vol%, respectively. The above calculation suggests the high collision frequency between SiC A–SiC B particles and SiC B–SiC B particles at SiC B fractions above 0.01 vol%. When two particles collide, the possibility of formation of flocculated particles is controlled by the interaction energy between charged particles. Eqs. (5)–(9) represent the van der Waals energy (E_a, Eqs. (5) and (6)) and repulsive energy (E_r, Eqs. (7)–(9)) to calculate the interaction energy ($E_i = E_a + E_r$) [16]. Eqs. (5), (7) and (8) are applied to calculate the interaction energy between same kinds of particles (A–A particles and B–B particles). Eqs. (7) and (8) are effective for the conditions of D (particle diameter) $\gg 1/\kappa$ (double layer thickness) and $D \ll 1/\kappa$, respectively. Eqs. (6) and (9) are used to calculate the interaction energy between different kind of particles (A–B particles).

$$E_a = -\frac{A}{12}\left[\frac{D^2}{H^2+2DH} + \frac{D^2}{(H+D)^2} + 2\ln\frac{H^2+2DH}{(H+D)^2}\right] \tag{5}$$

$$E_a = -\frac{Ar_1r_2}{6(r_1+r_2)H} \tag{6}$$

$$E_r = 32\pi\varepsilon\varepsilon_0\left(\frac{D}{2}\right)\left(\frac{RT}{ZF}\right)^2\tanh^2\left(\frac{ZF\varphi}{4RT}\right)\ln\{1+\exp(-\kappa H)\} \tag{7}$$

$$E_r = \frac{\pi\varepsilon\varepsilon_0 D^2\varphi^2}{H+D}\exp(-\kappa H) \tag{8}$$

$$E_r = \frac{\pi\varepsilon\varepsilon_0 r_1 r_2}{r_1+r_2}(\varphi_1^2+\varphi_2^2)\left[\frac{2\varphi_1\varphi_2}{\varphi_1^2+\varphi_2^2}\ln\left\{\frac{1+\exp(-\kappa H)}{1-\exp(-\kappa H)}\right\} + \ln\{1-\exp(-2\kappa H)\}\right] \tag{9}$$

The symbols in above equations express the following meaning: A the Hamaker constant, r_1 and r_2 the radius of particles 1 and 2, respectively, H the distance between particles 1 and 2, ε the relative dielectric constant of solution (78.3 for H_2O at 25 °C), ε_0 the permittivity of vacuum (8.8542×10^{-12} F/m), φ the surface potential (approximated by zeta potential) of charged particles, R the gas constant, F the Faraday constant, Z the charge number of electrolyte (assumed to be +1) and T the temperature (assumed to be 298 K). The double layer thickness ($1/\kappa$) was calculated to be about 100 nm for a typical electrolyte condition ($Z = +1$) of 10^{-5} mol/l. The interaction energy between SiC A–SiC A particles ($D = 800$ nm, $A = 10.9 \times 10^{-19}$ J [17], $\varphi = -34.2$ mV [2]) was calculated from Eqs. (5) and (7) ($D \gg 1/\kappa$). The interaction energy between SiC B–SiC B particles ($D = 30$ nm, $A = 10.7 \times 10^{-19}$ J [18], $\varphi = -29.8$ mV [2]) was calculated from Eqs. (5) and (8) ($D \ll 1/\kappa$). Similarly, Eqs. (6) and (9) were used to calculate the interaction energy between SiC A and SiC B ($A = \sqrt{A(\mathrm{SiC\ A})}\sqrt{A(\mathrm{SiC\ B})} = 10.8 \times 10^{-19}$ J) [19].

Fig. 2 shows three kinds of interaction energies, $E_a + E_r$, for the bimodal particles system of SiC A and SiC B. A small interaction energy was calculated between SiC B and SiC B or between SiC A and SiC B, as compared with the interaction energy between SiC A and SiC A. The formation of flocculated particles is accelerated under the condition of $E_i(max) < 15kT$ (=6.17×10^{-20} J at 298 K) [16]. The $E_i(max)$ values for the interaction of SiC B–SiC B particles and SiC A–SiC B particles were calculated to be 4.02×10^{-20} J ($H(max) = 6.15$ nm) and

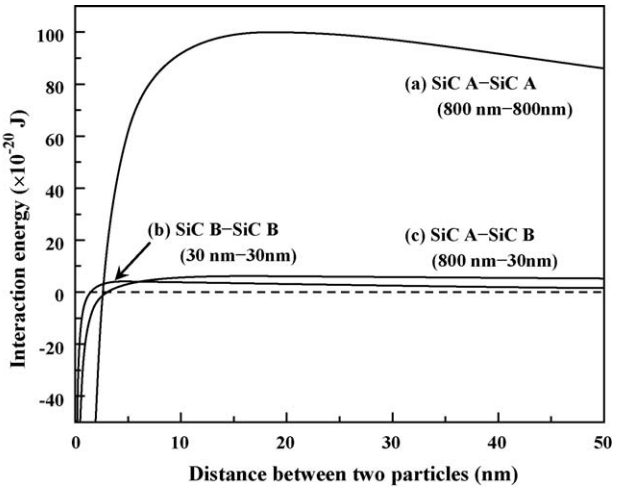

Fig. 2. Interaction energy of SiC-SiC particles as a function of distance between two particles.

6.32×10^{-20} J ($H(max) = 21.7$ nm), respectively. These values were comparable to the above condition for the formation of flocculated particles. The calculated results in Figs. 1 and 2 lead to the following prediction. In a solution at pH 7, SiC A particles are well dispersed because of the strong repulsive interaction. Addition of a small amount of SiC B to SiC A increases the collision frequency between SiC B–SiC B particles and SiC A–SiC B particles. The collision between particles form flocculated particles because of the significantly weak repulsive interaction energy. As a result, the above bimodal particles system forms a flocculated suspension through the bridging effect of SiC B particles.

3. Experimental procedure

A high purity α-SiC powder (powder A) supplied by Yakushima Electric Industry Co. Ltd., Kagoshima, Japan (specific surface area 13.4 m^2/g, median size 800 nm, true density 3.23 g/cm^3) and a plasma CVD–processed β-SiC powder (powder B) supplied by Sumitomo Osaka Cement Co. Ltd., Tokyo, Japan (specific surface area 50.9 m^2/g, median size 30 nm, true density 3.10 g/cm^3) were used in this experiment. Powders A and B were mixed at an interval of 10 vol% SiC B. These mixed particles were dispersed at 5 vol% solid in an aqueous solution at pH 7.0. The zeta potential of powders A and B was measured at a constant ionic strength of 0.01 M – NH_4NO_3 (Rank Mark II, Rank Brothers Ltd., Cambridge, UK). The rheological behavior of the mixed powder suspensions was measured by a cone and plate type viscometer (DV−II + Pro, Brookfield Eng. Lab., MA, USA). The prepared suspensions were consolidated through a plastic filter with a 20 μm pore diameter and three sheets of a membrane filter with a 0.1 μm pore diameter, which were attached to the bottom of the piston (polymeric resin, cross-sectional area 3.14 cm^2) moving at a constant crosshead speed of 0.2 mm/min. When the suspension in a closed cylinder was compressed by the piston, the filtrate flowed into and through the pore channels formed in the upper piston. The applied load and the height of the piston were continuously recorded (Tensilon RTC, A & D Co. Ltd., Tokyo, Japan). The consolidated SiC compact was taken out of the cylinder and dried at 100 °C in air for 24 h. The dried compact was heated at 1000 °C in Ar atmosphere for 1 h to give an enough strength for the measurement of bulk density by the Archimedes method using kerosene.

4. Results and discussion

4.1. Rheology of SiC suspensions of bimodal particles system

Fig. 3 shows typical shear rate-shear stress relations for the suspensions of bimodal SiC particles of 5 vol% solid. The measured shear stress increased with increasing shear rate and with the volume fraction of SiC B. This result was well understood by the calculated tendency in Figs. 1 and 2. The well dispersed SiC A suspension provided the very low shear stress but the agglomerated SiC B suspension needed a higher shear stress at a similar shear rate. The measured shear rate (γ)–shear stress (S) relations were analyzed by the following equations.

$$\text{Newtonian flow} \quad S = k\gamma \quad (k > 0) \tag{10}$$

$$\text{Bingham flow} \quad S = S_0 + k\gamma \quad (k > 0) \tag{11}$$

$$\text{Pseudoplastic flow} \quad S = S_0 + k_1\gamma^{1/2} + k_2\gamma \quad (k_1 > 0,\ k_2 \neq 0) \tag{12}$$

S_0 and k are constants. The condition of $k_1 = 2k_2^{1/2}S_0^{1/2}$ in Eq. (12) provides Eq. (13) known as Casson's equation.

$$S^{1/2} = S_0^{1/2} + k_2^{1/2}\gamma^{1/2} \tag{13}$$

The solid lines in Fig. 3 correspond to Eq. (12) and express well the nature of the measured data. The correlation coefficient of the curve in Fig. 3 was 0.987–0.999.

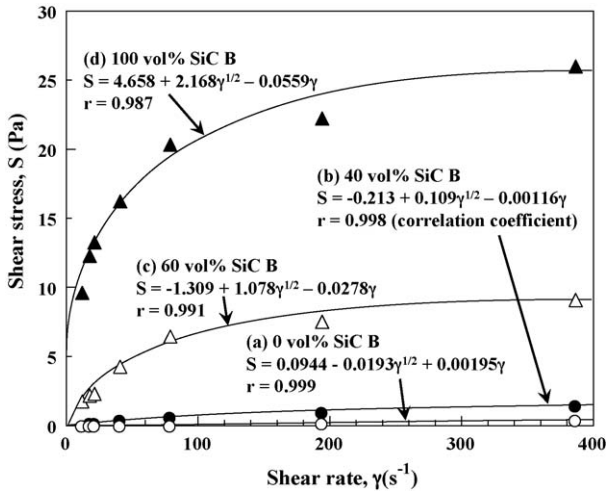

Fig. 3. Typical shear rate–share stress relations for mixed powder SiC suspensions. The solid lines represent Eq. (12) for pseudoplastic flow.

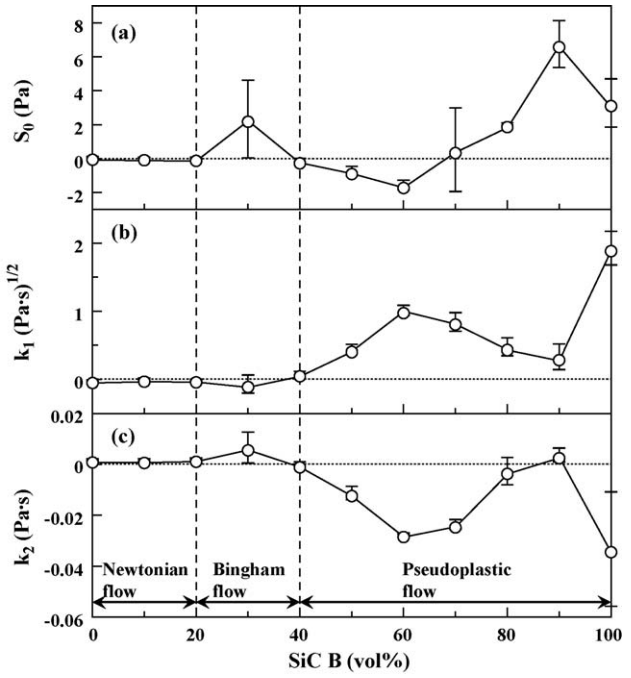

Fig. 4. Experimental constants S_0, k_1 and k_2 of Eq. (12) for pseudoplastic flow.

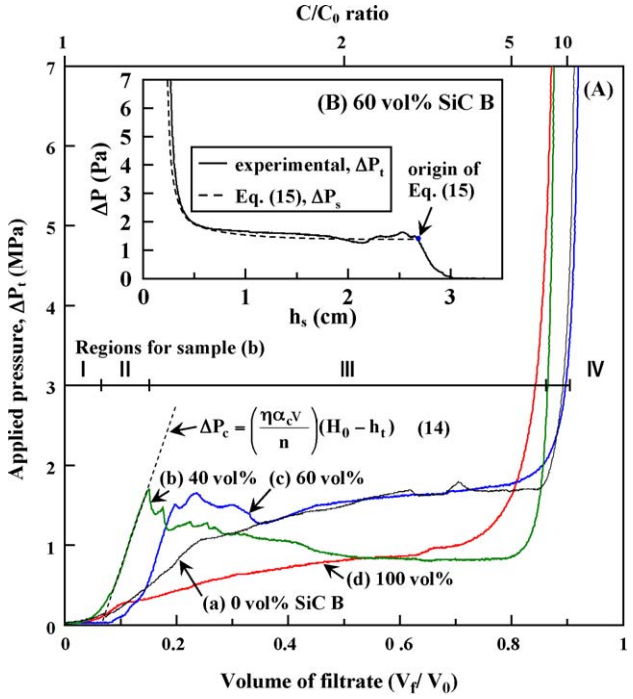

Fig. 5. Applied pressure (ΔP_t) as a function of volume of filtrate of mixed powder SiC suspension. ΔP_c in (A) represents the theoretical pressure drop across the consolidated cake during the pressure filtration of well dispersed particles. (B) The comparison between experimental result (ΔP_t) and theoretical pressure drop (ΔP_S, Eq. (15)) for the consolidation of flocculated suspension.

Fig. 4 shows S_0, k_1 and k_2 in Eq. (12) as a function of volume fraction of SiC B. The flow behavior of the bimodal particles suspension was divided in three regions. The region I at 0–20 vol% SiC B can be identified as Newtonian flow because k_1 and S_0 were close to 0. In region II at 20–40 vol% SiC B, k_1 was close to 0 but S_0 and k_2 had positive values, corresponding to Bingham flow. The rheological behavior in region III at 40–100 vol% SiC B is interpreted as a pseudoplastic flow.

4.2. Pressure filtration of SiC suspensions of bimodal particles

Fig. 5(A) shows the relationships between applied pressure (ΔP_t) and normalized filtrate volume (V_f/V_0, where V_f is the volume of filtrate during the period time of t, V_0 the volume of initial suspension) for bimodal SiC particles. The following four regions appeared [4]. Region I: a very low applied pressure at the initial stage of compression of the suspension. Region II: a linear increase of ΔP_t with increasing V_f. Region III: an almost plateau region of ΔP_t with increasing V_f. Region IV: a rapid increase of ΔP_t with a small increase of V_f. The consolidation behavior of bimodal SiC particles was analyzed based on the following filtration model of dispersed particles [4,20].

$$\Delta P_c = \left(\frac{\eta\alpha_c v}{nA}\right) V_f = \left(\frac{\eta\alpha_c v}{n}\right)(H_0 - h_t) \tag{14}$$

ΔP_c in Eq. (14) is the pressure drop across the consolidated cake of dispersed particles, η the viscosity of the filtrate, α_c the specific resistance of the consolidated cake, v the crosshead speed of piston, n the system parameter (=$(1 - C_0 - \varepsilon_c)/C_0$, C_0: initial volume fraction of colloidal particles, ε_c: porosity of the consolidated cake), A the cross-sectional area of the piston, H_0 the initial height of the piston, h_t the height of the piston (summation of h_c (height of the consolidated cake) and h_s (height of the colloidal suspension containing dispersed particles at time t)). When only the solution was compressed at the crosshead speed of $v = 0.5$ mm/min, the pressure drop across the filters (ΔP_m) was 5 ± 5 kPa. This value of ΔP_m was very small as compared with the experimental pressure range ΔP_t (=$\Delta P_c + \Delta P_m$) = 0.1 − 19 MPa, and ΔP_m can be neglected to ΔP_c. The small ΔP_c in region I reflects a small α_c for a thin consolidated layer. The linear increase of ΔP_c with V_f in region II is well interpreted by Eq. (14). However, the slope of the $\Delta P_t - V_f$ curve decreased when the consolidation process shifted to region III. No leak of the filtrate at the filters of the apparatus was recognized. The critical applied pressure corresponding to the start of region III was determined as a pressure at the boundary of regions II and III. In our previous papers [4,5], it was clarified that a phase transition from a dispersed suspension to a flocculated suspension occurs at a critical applied pressure (ΔP_{tc}) for nanoparticles 20–800 nm in size. The pressure drop ΔP_s for the consolidation of an initially flocculated suspension is calculated by Eq. (15)

$$\Delta P_S = \eta v B S^2 (H_0 C_0)^2 \int_{H_0}^{h_s} \frac{h_s}{(h_s - H_0 C_0)^3} dh_s \tag{15}$$

where B is the ratio of the shape factor to the tortuosity constant and S the ratio of the total solids surface area to the apparent

volume of the consolidated system. The integration of the right term, named as $T(h_s)$, is given by Eq. (16).

$$T(h_s) = \frac{1}{2}\left[\frac{H_0}{{H_0}^2(1-C_0)^2} - \frac{h_s}{(h_s - H_0C_0)^2} + \frac{1}{H_0(1-C_0)} - \frac{1}{h_s - H_0C_0}\right] \quad (16)$$

Fig. 5(B) shows the comparison of $\Delta P_t - h_t$ relation between experimental result and Eq. (15) for 40 vol% SiC A–60 vol% SiC B suspension. The origin (H_0) of Eq. (15) was shifted to the height (h_{sc}) of the suspension corresponding to ΔP_{tc}. The height of h_{sc} was calculated by $h_{sc} = V_{fc}/nA$, where V_{fc} was the critical volume of filtrate at ΔP_{tc} and n was estimated from the final packing density of particles at 19 MPa. The measured $\Delta P_t - h_t$ curve was well fitted by Eq. (15) for the flocculated suspension model. Therefore, the consolidation behavior of bimodal particles system was well explained by the combination of two filtration models for well dispersed particles in early stage and for flocculated particles in latter stage.

4.3. Phase transition pressure and packing density of bimodal SiC particles

Fig. 6 shows phase transition pressure (ΔP_{tc}), concentration at ΔP_{tc} and packing density of bimodal particles after calcination at 1000 °C in Ar atmosphere. ΔP_{tc} was almost constant in the fraction range of SiC B at 0–60 vol% (ΔP_{tc} = 0.72–1.11 MPa) and at 60–100 vol% (ΔP_{tc} = 0.11–0.58 MPa), respectively. This result suggests that the phase transition to a flocculated suspension occurs under a low applied pressure in a SiC B–rich suspension (SiC B > 60 vol%). The concentration at ΔP_{tc} decreased at a higher content of SiC B particles but almost constant in a wide range of SiC B from 30 to 100%. The comparison between rheological behavior in Fig. 4 and ΔP_{tc} in Fig. 6(a) suggests that ΔP_{tc} becomes a lower value for a pseudoplastic flow suspension rather than for a Newtonian flow or Bingham flow suspension. As explained for the result of Fig. 2, the bridging effect of SiC particles in a pseudoplastic flow suspension becomes significant, resulting in the decreased ΔP_{tc}. After the phase transition to a flocculated suspension, the particle concentration of the suspension increases during the filtration. Packing density of calcined compacts decreased at a higher fraction of SiC B particles. The packing behavior of mixed SiC particles was analyzed by applying the concept of partial molar volume for the mixed powder system. The partial molar volume ($\bar{V}$) of each powder is given by Eqs. (17) and (18),

$$\bar{V}_A = V - X_B\left(\frac{dV}{dX_B}\right) \quad (17)$$

$$\bar{V}_B = V + (1 - X_B)\left(\frac{dV}{dX_B}\right) \quad (18)$$

where X_B is the molar fraction of powder B in the mixed powder system and V the molar volume of mixed powder compact which can be determined from bulk density. Fig. 7 shows the molar volume of bimodal SiC particles consolidated. The measured data were fitted by the polynominal approximation by Eq. (19),

$$V = a + bX_B + cX_B^2 + dX_B^3 + eX_B^4 \quad (19)$$

where a–e are experimental constants. As seen in Fig. 7, the two intercept values of tangent line for an arbitrary composition of SiC B correspond to $\bar{V}_A$ and $\bar{V}_B$. Fig. 8(a) shows $\bar{V}_A$ and $\bar{V}_B$ as a function of X_B. $\bar{V}_B$ was larger than $\bar{V}_A$ and approached a constant value at X_B = 0.5–1.0. As compared with $\bar{V}_B$, $\bar{V}_A$ was not sensitive to X_B. This analysis indicates that (1) molar

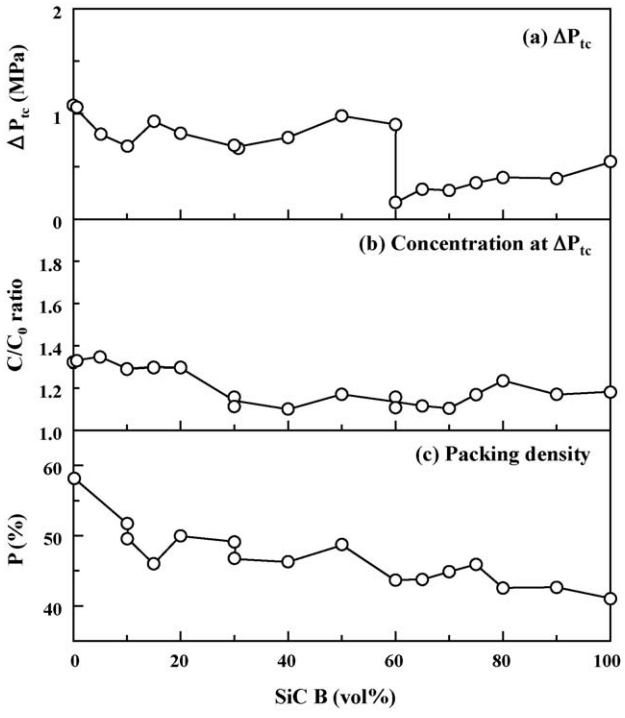

Fig. 6. (a) Phase transition pressure (ΔP_{tc}), (b) concentration at ΔP_{tc} and (c) packing density for mixed powder system.

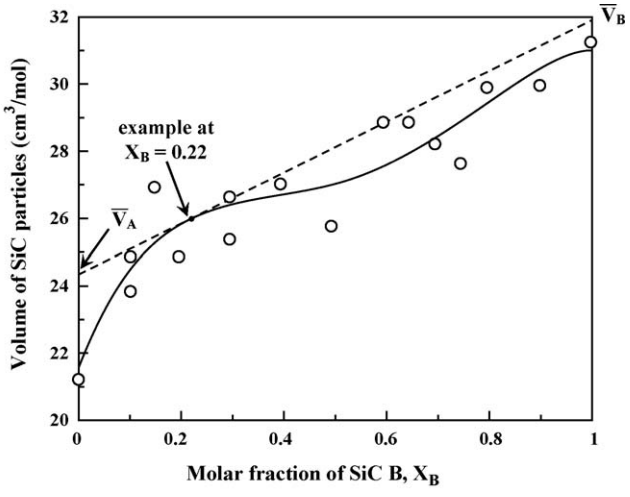

Fig. 7. Analysis of partial molar volume of SiC A and SiC B particles in the mixed powder compact after calcination at 1000 °C.

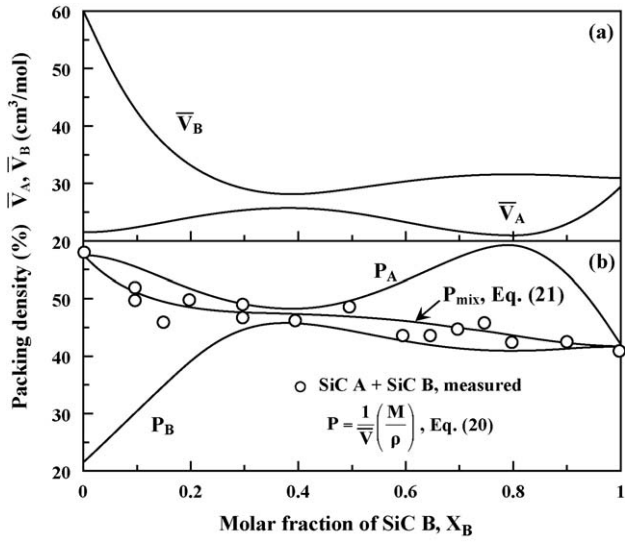

Fig. 8. Partial molar volume (a) and packing density (b) of SiC particles A and B in the mixed powder compact.

volume of SiC depends on particle size and (2) finer particles of 1 mol SiC occupy a large volume in the mixed powder system. The packing density (P) of each powder in the mixed powder compact is related to $\bar{V}$ by Eq. (20),

$$P = \frac{1}{\overline{V}}\left(\frac{M}{\rho}\right) \tag{20}$$

where M is the molecular weight and ρ the true density of particles. Fig. 8(b) shows P values of SiC A and SiC B particles. It is apparent that the larger particles are densely packed than smaller particles in the mixed powder system. The packing density of bimodal particles system (P_{mix}) is given by Eq. (21),

$$P_{mix} = \frac{1}{\rho_m}\frac{1}{(X_A/P_A\rho_A) + (X_B/P_B\rho_B)} \tag{21}$$

where ρ_m is the true density of mixed powders. The measured density of mixed powder system was well expressed by Eq. (21) based on the partial molar volume of each powder. The structure formed by the connection between larger particles is dense but that formed by the connection between smaller particles is porous. These characteristics of packing structures are reflected in the measured density of mixed powder system.

Fig. 9 shows the schemes of structures estimated from packing density shown in Fig. 8(b). The structure of SiC A particles is close to simple cubic packing (density 52.4%) at $X_B = 0.2$. The fine SiC B particles are packed in the pores formed by SiC A particles or cover the surfaces of SiC A particles. Further addition of SiC B particles (30–40 mol% SiC B) expands the structure of SiC A particles, resulting in the decreased packing density of A particles, P_A. The increased number of SiC B particles changes the porous structure (Fig. 9(a)) to dense one (Fig. 9(b)). In the range of $X_B = 0.5$–0.8, P_A was in the range of 0.498–0.593. This packing density reflects the mixed structure of simple cubic packing and random close packing (calculated density of random close packing: 63.7%) or body-centered cubic packing (theoretical packing density: 68.0%). P_B value is around 0.41 and SiC B particles are porously packed. Further addition of SiC B particles ($X_B = 0.9$) leads to the decreased packing density of SiC A particles. Little change of packing density was measured

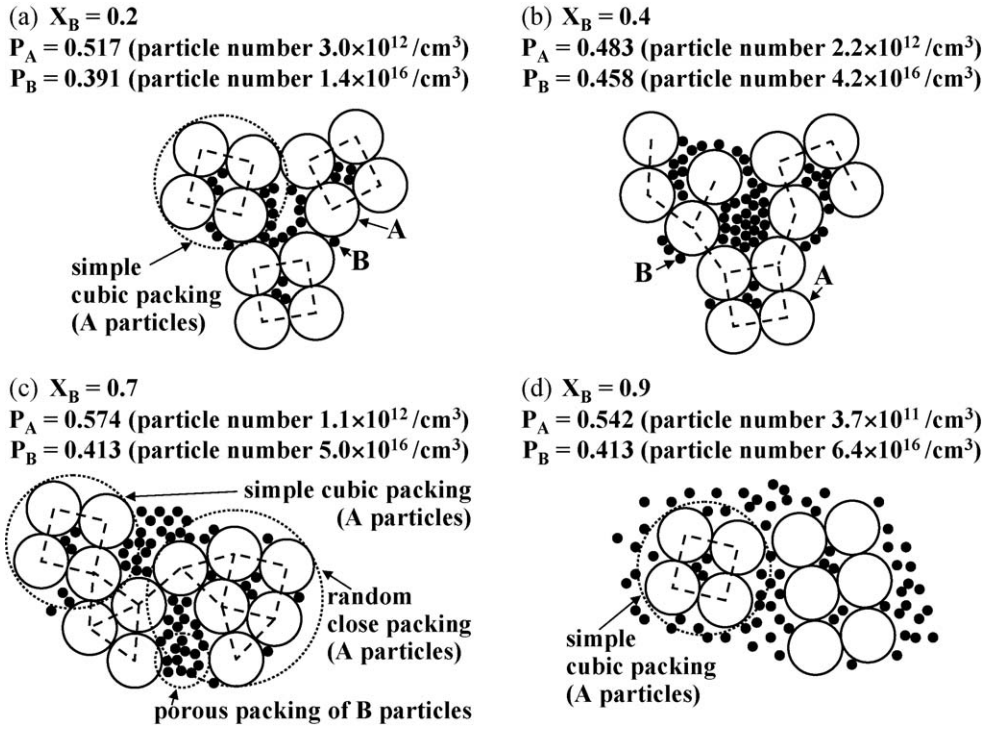

Fig. 9. Schematic structures estimated from packing density of SiC particles A and B.

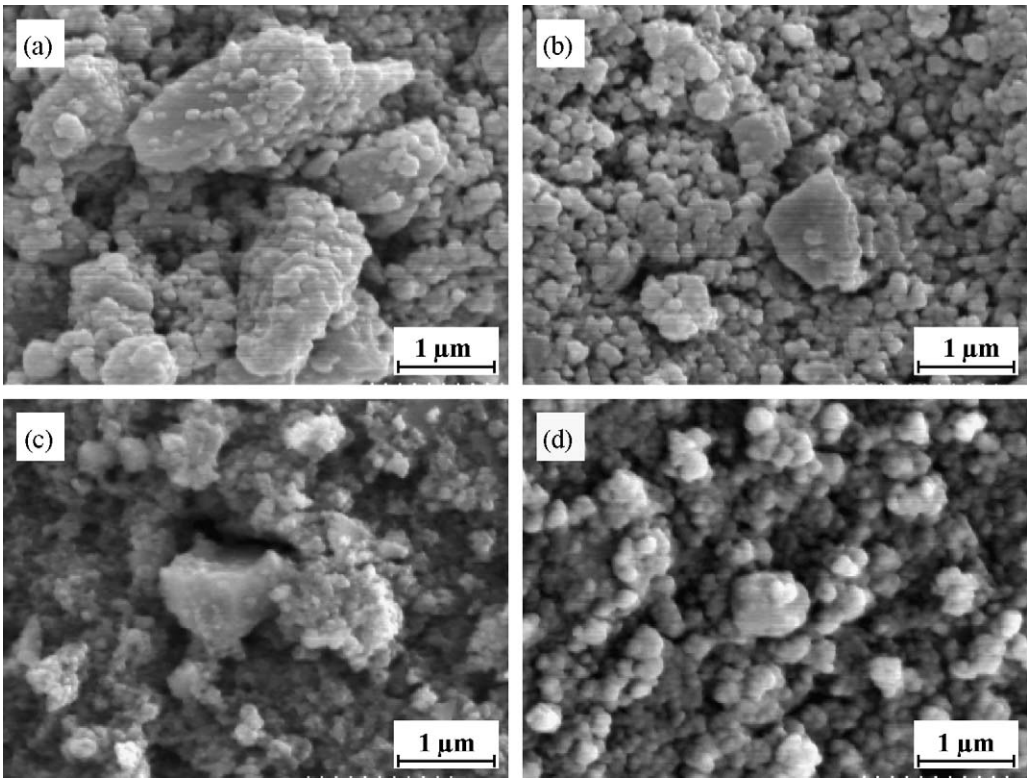

Fig. 10. Microstructures of SiC compacts with (a) 20 vol% SiC B, (b) 40 vol% SiC B, (c) 70 vol% SiC B and (d) 90 vol% SiC B after calcination at 1000 °C in Ar atmosphere.

for SiC B particles. As reported in Fig. 9, the packing structure formed by SiC A particles or SiC B particles is influenced by each other.

Fig. 10 shows the microstructures of SiC compacts after calcination at 1000 °C. At the composition of 20 vol% SiC B (Fig. 10(a)), the small SiC B particles were attached to the surface of large SiC A particles. This result is understood by the calculated interaction energy shown in Fig. 2. The observed microstructure was basically similar to the schematic structure shown in Fig. 9(a). In the microstructure for 40 vol% SiC B composition, it was difficult to see directly large A particles. The increased fraction of SiC B particles separates SiC A particles connected in Fig. 9(b). In addition, SiC B particles formed particle clusters because of the weak repulsive energy as shown in Fig. 2. When the fraction of SiC B particles is increased to 70 vol%, large SiC A particles were embedded in the matrix of SiC B particles. A similar microstructure was also observed for 90 vol% SiC B composition. From Fig. 10(d), it was difficult to see the structure formed by the connection between SiC A particles.

5. Conclusions

(1) The rheological behavior of the suspensions of bimodal SiC particles (800–30 nm) changed as follows with increasing fraction of 30 nm SiC particles: Newtonian flow → Bing-Bingham flow → pseudoplastic flow.
(2) Colloidal phase transition from dispersed to flocculated suspension occurred at a critical applied pressure (ΔP_{tc}) during the pressure filtration of the mixed powder suspensions. The ΔP_{tc} and final packing density decreased with an increase of the fraction of 30 nm SiC.
(3) Partial molar volume of large SiC particles was smaller than that of small SiC particles. Therefore, large SiC particles were more densely packed than small SiC particles in all the range of mixing.
(4) Understanding of the packing characteristics of small and large SiC particles assists an observer in interpreting the microstructures of SiC compacts.

References

[1] Y. Hirata, M. Nakamura, M. Miyamoto, Y. Tanaka, X.H. Wang, Colloidal consolidation of ceramic nanoparticles by pressure filtration, J. Am. Ceram. Soc. 89 (6) (2006) 1883–1889.
[2] K. Kishigawa, Y. Hirata, Forming of aqueous SiC suspension by pressure filtration, J. Ceram. Soc. Jpn. 114 (3) (2006) 259–264.
[3] K. Kishigawa, Y. Hirata, Packing density and consolidation energy of flocculated aqueous SiC suspension, J. Eur. Ceram. Soc. 26 (1–2) (2006) 217–221.
[4] Y. Hirata, Y. Tanaka, Pressure filtration model of ceramic nanoparticles, J. Am. Ceram. Soc. 91 (3) (2008) 819–824.
[5] Y. Tanaka, Y. Hirata, N. Matsunaga, M. Nakamura, S. Sameshima, T. Yoshidome, Pressure filtration of nanometer-sized SiC powder, J. Ceram. Soc. Jpn. 115 (11) (2007) 786–791.
[6] C. Kaya, E.G. Butler, M.H. Lewis, Co-extrusion of Al_2O_3/ZrO_2 bi-phase high temperature ceramics with fine scale aligned microstructures, J. Eur. Ceram. Soc. 23 (6) (2003) 935–942.
[7] K.F. Cai, D.S. McLachlan, N. Axen, R. Manyatsa, Preparation, microstructures and properties of Al_2O_3–TiC composites, Ceram. Int. 28 (2) (2002) 217–222.

[8] G.J. Li, X.X. Huang, J.K. Guo, Fabrication and mechanical properties of Al_2O_3–Ni composite from two different powder mixtures, Mater. Sci. Eng. A 352 (1–2) (2003) 23–28.
[9] S. Sameshima, M. Ishizuka, Y. Yoshida, Y. Hirata, in: K. Niihara, S. Hirano, S. Kanzaki, K. Komeya, K. Morinaga (Eds.), Proceedings of the 6th International Symposium on Ceramic Materials & Components for Engines, 1998, pp. 446–451.
[10] N. Matsunaga, S. Ueno, Y. Tanaka, Y. Hirata, Colloidal consolidation of mixed powders of the alumina/indium tin oxide system, Ceram. Trans. 198 (2007) 153–158.
[11] Y. Koreeda, Y. Hirata, S. Sameshima, Analysis of microstructure of two-component powder compact by electrical conductivity measurement, J. Ceram. Soc. Jpn. 112 (5) (2004) S280–S285.
[12] Y. Koreeda, Y. Hirata, S. Sameshima, Analysis of microstructure of two-component powder compact by electrical conductivity measurement (part 2), J. Ceram. Soc. Jpn. 113 (8) (2005) 534–539.
[13] Y. Hirata, N. Numaguchi, W.H. Shih, Dispersion and consolidation of ceramic particles, Key Eng. Mater. 159–160 (1999) 127–134.
[14] Y. Hirata, W.H. Shih, Colloidal processing of two-component powder systems, in: P. Vincenzini (Ed.), Proceedings of the 9th CIMTEC—World Ceramics Congress & Forum on New Materials, Part B, 1999, pp. 637–644.
[15] J.T.G. Overbeek, in: H.R. Kruyt (Ed.), Colloid Science I, Elsevier Publishing Co., Asterdam, 1952, p. 278.
[16] Y. Hirata, Y. Tanaka, Characterization of colloidal suspension of ceramic nanoparticles, Bull. Ceram. Soc. Jpn. 42 (2) (2007) 87–92.
[17] R.H. French, Origins and applications of London dispersion forces and Hamaker constants in ceramics, J. Am. Ceram. Soc. 83 (9) (2000) 2117–2146.
[18] J.A. Lewis, Colloidal processing of ceramics, J. Am. Ceram. Soc. 83 (10) (2000) 2341–2359.
[19] J. Sum, B.V. Velamakanni, W.W. Gerberich, L.F. Francis, Aqueous latex/ceramic nanoparticle dispersions: colloidal stability and coating properties, J. Colloid Interface Sci. 280 (2) (2004) 387–399.
[20] I.A. Aksay, C.H. Schilling, Advances in ceramics, Forming of Ceramics, vol. 9, The American Ceramic Society, Columbus, OH, 1984, pp. 85–93.